Adsorption and Dissociation of *R*-Methyl *p*-Tolyl Sulfoxide on Au(111)

Mauro Satta, Nicola Zema, Stefano Turchini, Stefano Franchi, Giorgio Contini, Alessandra Ciavardini, Cesare Grazioli, Marcello Coreno, Monica de Simone, Massimo Tomellini, and Susanna Piccirillo*

ACCESS | Metrics & More | Article Recommendations | Supporting Information

ABSTRACT: Sulfur-based molecules producing self-assembled monolayers on gold surfaces have long since become relevant functional molecular materials with many applications in biosensing, electronics, and nanotechnology. Among the various sulfur-containing molecules, the possibility to anchor a chiral sulfoxide to a metal surface has been scarcely investigated, despite this class of molecules being of great importance as ligands and catalysts. In this work, (*R*)-(+)-methyl *p*-tolyl sulfoxide was deposited on Au(111) and investigated by means of photoelectron spectroscopy and density functional theory calculations. The interaction with Au(111) leads to a partial dissociation of the adsorbate due to S−CH₃ bond cleavage. The observed kinetics support the hypotheses that (*R*)-(+)-methyl *p*-tolyl sulfoxide adsorbs on Au(111) in two different adsorption arrangements endowed with different adsorption and reaction activation energies. The kinetic parameters related to the adsorption/desorption and reaction of the molecule on the Au(111) surface have been estimated.
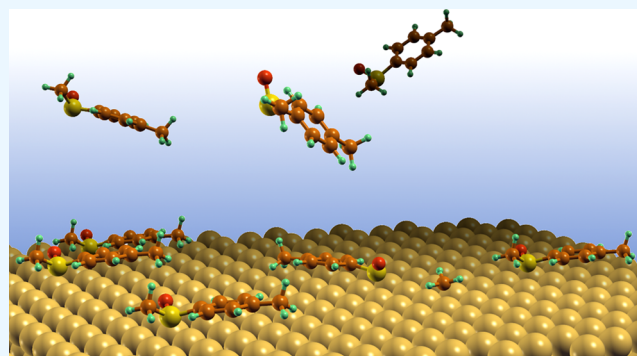
1. INTRODUCTION

The ability to develop self-assembled monolayers (SAMs) of organic molecules on solid surfaces and nanoparticles and the understanding of their structure are relevant issues for the design of molecular devices for future technological and biomedical applications.[1−5]

A particularly attractive case is constituted by the self-organization of chiral molecules, leading to a local or global surface chirality, with potential functionality for molecular recognition and selective chemical reactivity.[6−8] From a fundamental viewpoint, the description of the intermolecular bonding[9,10] and of the interactions with the substrate is a key issue for understanding the geometrical arrangement of these molecular aggregates as well as their electronic and chemical properties.[11−14]

As a matter of fact, SAMs of organosulfur compounds on gold surfaces are archetypal systems[15,16] that have been extensively studied and used to prepare structurally and chemically complex organic surfaces with distinct microscopic characteristics.[17,18] In particular, the deposition of thiol derivatives[17−21] has become the most simple and efficient way for the functionalization of gold substrates and nanoparticles,[22−28] with many applications as electric devices, biosensors, and catalysts.[1−5,28,29] Other alternatives to thiols, containing sulfur in the head group have been reported, including sulfides, disulfides,[15−17] thiosulfates,[30] thiocya-

nates,[31] sulfenyl chlorides,[32] sulfonyl phthalimides,[33] sulfonates,[34] and thiophene derivatives.[35−38]

At variance, monolayers of sulfoxides, compounds containing a substituted sulfinyl group (RR′S = O),[39] have gained much less attention despite the proven role of these molecules in organic synthesis, catalysis, pharmaceutical, or material chemistry.[40−42] Only few studies have been reported on the interaction of sulfoxides with gold[43−48] and almost all[43−47] are related to the adsorption on gold of dimethyl sulfoxide (CH₃SOCH₃), aimed at understanding how this widely used polar, aprotic solvent interacts with the metal surface.

Chiral sulfinyl compounds[49] are commonly used as chiral ligands/catalysts and in biologically active compounds.[41,42] The geometrical structure of a sulfoxide (RR′S = O, where R and R′ are two organic substituents bound to the sulfur atom of the SO sulfinyl group) is pyramidal. Hence, sulfoxides possess a stereogenic sulfur atom with a free electron pair, connected to an electronegative oxygen atom by a polar bond. Stable sulfoxide enantiomers are possible if R≠R′ and the

inversion barrier is sufficiently higher than thermal energy. Because of the relevance that chirally modified metal surfaces[6,50−53] have in many applications, such as heterogeneously catalyzed processes or chemical sensors, we considered it important to characterize the structure and electronic properties of a chiral sulfinyl compound deposited on a gold surface.

In this paper, we report a combined experimental and theoretical study to elucidate the primary binding mechanism of a small chiral aromatic sulfoxide, R-methyl p-tolyl sulfoxide (Metoso, Figure 1) deposited on Au(111) at room temper-
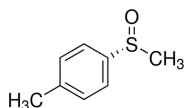

Figure 1. Structure of R-methyl p-tolyl sulfoxide (Metoso).

ature (RT) in ultrahigh vacuum (UHV). With the experimental conditions employed in this study the self-assembled monolayers are not obtained, allowing low surface coverages investigation of energetics and kinetics of isolated Metoso molecules on the Au(111) surface. Photoelectron spectroscopy (PES) investigation evidenced a partial dissociative adsorption of Metoso on the Au(111) surface. Density functional theory (DFT) calculations were performed to investigate the adsorption and decomposition reaction of Metoso on the Au(111) surface.

2. EXPERIMENTAL AND THEORETICAL METHODS

2.1. Experimental Methods. The experimental study was performed at the Materials Science Beamline and Gas Phase Photoemission beamline at the Synchrotron Light source Elettra, Trieste, Italy. R-Methyl p-tolyl sulfoxide with 99% purity was purchased from Sigma-Aldrich, transferred to a vial under dry nitrogen, and purified by means of several freeze−pump−thaw cycles. For gas-phase measurements, the sample was evaporated at 40 °C and the photoelectron spectra were acquired at a background pressure of 5×10^{-6} mbar. The gas-phase core-level photoelectron spectra were measured at 392 eV (C 1s), 632 eV (O 1s), and 260 eV (S 2p) photon energy with a total resolution (photon + analyzer) of 0.11, 0.35, and 0.06 eV respectively. The binding energy scale of the C 1s, O 1s, and S 2p photoelectron spectra were calibrated by using CO_2 (C 1s 297.7 eV,[54] O 1s 541.08 eV[55]) and SF_6 (S $2p_{3/2}$ 180.21 eV − S $2p_{1/2}$ 181.5 eV[56]) molecules.

The deposited samples were prepared according to the following procedure. The Au(111) crystal was cleaned by repeated cycles of Ar^{+}-ion sputtering and annealing at 470 °C and checked by LEED and core-level photoelectron intensities. Au(111) was exposed to Metoso by backfilling the preparation chamber ($P \sim 5 \times 10^{-8}$ mbar) through a leak valve connected to a glass vial. During deposition, the glass vial, inlet system, and leak valve were heated at 35 °C, while Au(111) was kept at RT. Deposition times were 30 and 60 min in two independent exposures. PES data were acquired in a normal electron emission geometry by a Specs Phoibos 150 hemispherical electron energy analyzer with $\pm 8°$ acceptance angle and with photon energies of 300 eV (S 2p), 410 eV (C 1s), and 650 eV (O 1s) with 15 eV pass energy. The binding energy scale of the photoelectron spectra was calibrated by the Fermi edge.

2.2. Computational Details. The quantum modeling has been carried out with the QUANTUM ESPRESSO simulation package[57] within the Kohn−Sham version of density functional theory (DFT). Perdew−Burke−Ernzerhof (PBE) exchange−correlation functional ultrasoft pseudopotentials have been used, and Kohn−Sham valence states were expanded in a plane-wave basis set with a cutoff of 340 eV for the kinetic energy. The energy threshold has been fixed at 10^{-5} eV and a mixing factor for self-consistency of 0.7 were employed to obtain the self-consistency of the electron density. For Brillouin-zone integration in metals, a Gaussian spreading of 0.06 Ry has been used, as well as Marzari−Vanderbilt smearing and the local-density-dependent Thomas−Fermi screening have been used for the electron mixing mode. Integration in the reciprocal space was performed using the γ point after preliminary test calculations with a Monkhorst−Pack automatically generated uniform grid of 16 k-points have been tested on dimethyl sulfoxide on Au(111) showing an error less than 0.05 eV for adsorption energy and less than 0.01 eV for the O 1s core-level shift. The geometry optimization was calculated within the conjugate gradients scheme, with a threshold of 0.01 eV[−1] on the Hellmann−Feynman forces on atoms. The coordinates of the gold atoms of the third layer below the surface have been fixed at their bulk values.

Calculations were performed using a primitive orthogonal unit cell containing 90 Au atoms. We used a cell dimension a = 14.9538 Å, b = 14.3893 Å, and a height of 20 Å to minimize the vertical surface interactions among replicated cells.

The shift of the binding energy of the core electron in the 1s orbital of the oxygen atoms has been computed as the difference of the total energy calculated using a pseudopotential generated in the corresponding core-level hole for the O atom of Metoso adsorbed on Au(111) or in gas phase.

The interaction between organic molecules and metal surfaces can be treated with good accuracy by employing DFT with vdW corrections. Standard vdW corrections are known often to overestimate the long-range interactions occurring between organic molecules and metal surfaces.[58] In the present calculations, the S6 parameter of Grimme,[59] which controls the strength of the vdW interactions, has been fixed at 0.2 in order to correctly reproduce the experimental adsorption energies of specific molecules on Au(111), which have the functional groups of Metoso: benzene, CH_3SH, CH_3OH, and SO_2 (see Table 1).

Table 1. Effects on the Adsorption Energies (ΔE) due to the Rescaling of the Dispersion Parameter S6[a]

	ΔE_{calc} (eV)	ΔE_{exp} (eV)
benzene	0.69	0.64[60]
CH_3SH	0.77	>0.5−0.6[61]
CH_3OH	0.44	0.42[62]
SO_2	0.56	0.34[63]

[a]Calculated and experimental ΔE for molecules on Au(111) with functional groups related to Metoso with S6 = 0.2.

3. RESULTS

3.1. Core-Level Photoelectron Spectra of Metoso Deposited on Au(111). Figure 2a,b shows a series of S 2p core-level spectra taken at different times after exposure to Metoso at RT for 30 min (Figure 2a) or 60 min (Figure 2b) depositions. The spectra have been acquired in a sequence
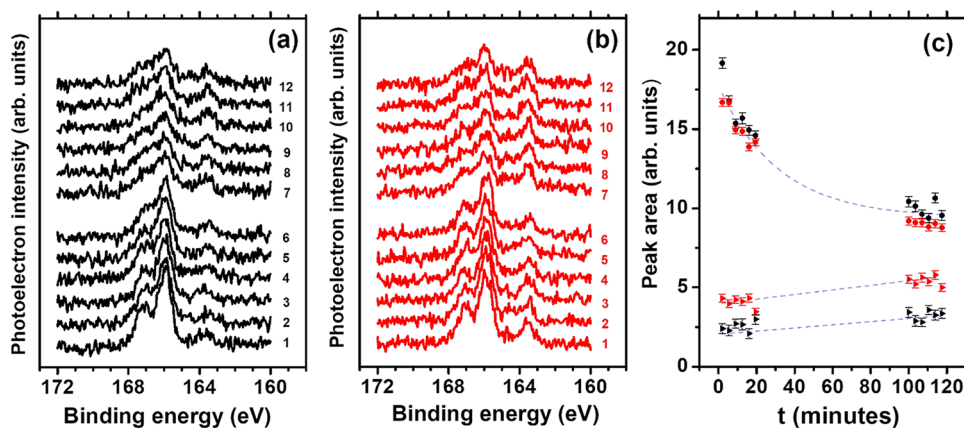
Figure 2. Photoelectron spectra of the S 2p region taken with 300 eV photon energy at different time delays after sample exposure. Each curve is the average of five consecutive scans, lasting in total 210 s. The numbers on the right indicate acquisition order. The first series of spectra (1−6 bottom curves) have been acquired in succession soon after exposure and the second series (7−12 top curves) about 100 min later. Background has been subtracted and spectra are vertically displaced. (a) Au(111) exposition to Metoso for 30 min; (b) Au(111) exposition to Metoso for 60 min; (c) temporal evolution of the signals area of the two S 2p doublets, with $2p_{3/2}$ component at 165.9 eV (circles) and 163.5 eV (triangles) for 30 min exposure to Metoso (black) and for 60 min exposure to Metoso (red). The blue dashed lines serve only to guide the eye.
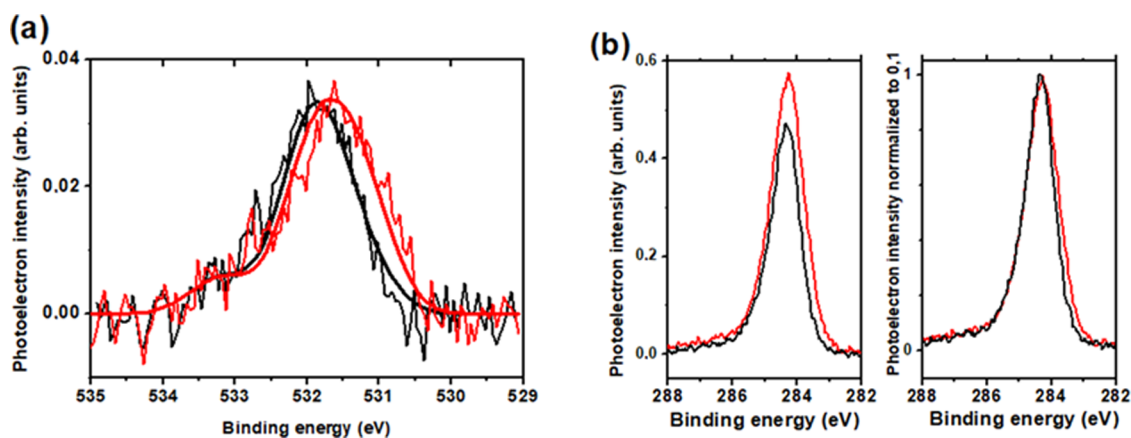

Figure 3. PES spectra of Metoso deposited on clean Au for 30 min (black lines) and 60 min (red lines). (a) O 1s region for a 650 eV photon energy with total fitted area (see text and the Supporting Information for details). (b) C 1s region for a 410 eV photon energy; left: absolute intensities, right: intensities normalized from 0 to 1.

lasting 20 min soon after exposure (Figure 2a,b, 1−6 bottom curves) and in the same way about 100 min later (Figure 2a,b, 7−12 top curves).

The spectra have been fitted with pseudo-Voigt functions (see Figure S1) and present two doublets, with the $2p_{3/2}$ components at 165.9 and 163.5 eV, the principal and smaller, respectively. We assign the higher BE component at 165.9 eV to the intact adsorbed Metoso molecule, while the lower BE one at 163.5 eV can be associated with a product of the dissociation of Metoso.

In the Supporting Information, the gas-phase PES spectra of Metoso in the S 2p, C 1s, and O 1s binding energy regions are reported (Figure S2). In particular, Figure S2a shows the S 2p photoelectron spectra taken at 260 eV photon energy, where only one S 2p doublet (1.19 eV spin−orbit splitting and a 2:1 branching ratio) is present. For the gas-phase measurements, the temperature of the Metoso inlet system was slightly higher (40 °C) than the temperature (35 °C) employed during the deposition of Metoso on Au(111). The presence of only one S 2p core-level doublet in the gas-phase Metoso spectrum indicates that the molecules do not decompose during the

evaporation, yet dissociation results from the interaction with Au(111).

Since in a previous study,[47] minor features at about 163 eV in the S 2p spectra of dimethyl sulfoxide deposited on Au(111) were ascribed to radiation damage, we checked for this possibility. As shown in Figure 2a,b, the signal at 163.5 eV is already present at the beginning of the PES acquisitions on the sample. We also systematically checked for damage at the end of the sets of photoelectron measurements. Figure S3 reports the S 2p spectra acquired after about 2 h in surface regions that have been repeatedly irradiated and S 2p spectra acquired in different nonirradiated areas. Almost no difference of the intensity and energy position of the S 2p doublets has been observed, indicating that we can rule out radiation damage.

Figure 2c reports the area of the S 2p signal for intact ($A_{165.8\,eV}$) and fragmented ($A_{163.4\,eV}$) Metoso as a function of time for the two exposures to Metoso (30 min shown in black and 60 min shown in red). For both depositions, it can be seen that the area of the S 2p signal associated with the intact Metoso molecule (black or red circles) is not dissimilar for the two samples and decreases over time. The area of the signal at 163.5 eV is lower in the case of 30 min deposition (black
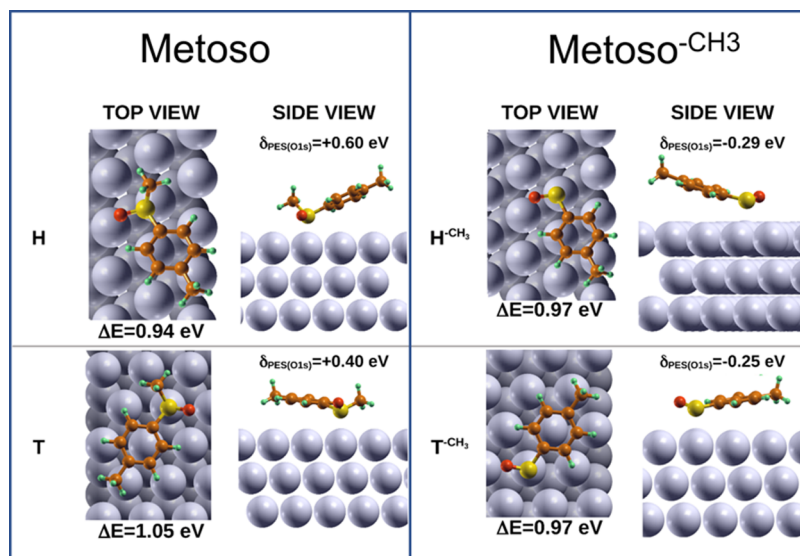
Figure 4. Structure and energetics of Metoso and Metoso$^{-CH_3}$ monomers adsorbed on Au(111). Gray: Au atoms, yellow: S atom, red: O atom, dark brown: C atoms, green: hydrogen atoms. ΔE refers to the adsorption energy and $\delta_{\text{PES(O 1s)}}$ to the shift of the O 1s core-level binding energy with respect to that of the free molecule in the gas phase.

triangles), with respect to 60 min deposition (red triangles). If we compare the spectra acquired shortly after exposure, spectra numbered 1 in Figure 2a (30 min exposure) and Figure 2b (60 min exposure), an area ratio $A_{166.0 \text{ eV}}/A_{163.5 \text{ eV}}$ of 8.0 is obtained for 30 min and of 3.7 in the case of 60 min deposition. In both samples, a slight increase of the area intensity as a function of time of the signals associated with the dissociation of the molecules (black o red triangles in Figure 2c) is observed.

Figure 3a displays the photoelectron spectra in the O 1s region, taken about 50 min after Metoso deposition. A broad band centered around 532.0 eV of BE was observed for O 1s of Metoso exposed for 30 min (Figure 3a, black line). The lineshape of the O 1s exposed for 60 min (Figure 3a, red line) is different, and it appears to have a higher contribution from a lower-binding-energy component, which shifts the band toward lower binding energy values. The bands have been fitted as discussed in more detail in Section 4. The total fitted area is shown in Figure 3a, while the individual gaussian components are shown in Figure S4.

Figure 3b shows the spectra of the C 1s, taken about 30 min after sample preparation. It can be observed that the intensity of the C 1s signal is lower in the case of 30 min exposition (Figure 3b, left, black line) with respect to 60 min exposition (Figure 3b left, red line), and the lineshape of the latter is slightly broadened in the lower BE side, as evident from the spectra normalized from 0 to 1 reported in Figure 3b, right.

The Au 4f core-level spectra obtained for the clean Au(111) surface and for the two different expositions to Metoso are reported in Figure S5. The intensities of the Au 4f signal are higher for the sample exposed to Metoso for 30 min with respect to the sample exposed for 60 min. An estimation of the surface coverage, in terms of the ratio between the density of S atoms on the surface and that of Au at the outermost Au(111) surface was attained from the total area ratio of the S 2p and Au 4f PES signals, as described in ref 64 and reported in Supporting Information. For the sample exposed to Metoso for 60 min, the surface coverage resulted around 0.01, while for the sample exposed to Metoso for 30 min, the coverage is slightly lower, 0.008. Considering the number of molecules per

surface gold atom (from DFT calculation, on account of the area occupied by a molecule, Figure 4) to be about 1:10, it is possible to estimate that the data presented are referred to 0.08−0.1 ML (1 ML is defined as a saturated surface).

It should be pointed out that these values are attained from the Au 4f and S 2p spectra, both of them available around 100 min after sample transfer. The low values obtained indicate a submonolayer range for the deposition at RT. Moreover, an eventual contribution of molecules forming multilayers would have resulted in a shift of the peak maxima in the S 2p spectra[46,47] acquired at different deposition and/or acquisition times, which we do not observe.

3.2. Adsorption and Dissociation of Metoso on Au(111). From the photoemission data, we infer that nondissociated Metoso is present on Au(111) together with products originating from its dissociation due to interaction with the gold surface. The most labile bond in the molecule is the S−CH$_3$ bond and homolytic dissociation of this bond results in the formation of the p-tolyl sulfinyl (Metoso$^{-CH_3}$) and methyl (CH$_3$) radicals.

We have calculated the minimum energy path (B3LYP/6-31++g**) for the dissociation of this bond in the gas phase, which results to be endothermic by 1.61 eV and barrierless along the reaction coordinate. The reaction energy on the Au(111) surface can be estimated from the calculated adsorption energies of reactant and products. At variance with the gas phase, on the gold surface, an activation barrier for the reaction is expected.

Figure 4 reports the most stable calculated structures of Metoso and Metoso$^{-CH_3}$ interacting with the Au(111) surface. The optimization of the structure of a Metoso molecule on Au(111) gives two different adsorption arrangements depending on the position of the aromatic ring with respect to the surface Au atoms. The aromatic ring can have its center on a top (indicated below as T conformation) or hollow (indicated below as H conformation) site on Au(111). H conformation has lower adsorption energy ($\Delta E = 0.94$ eV) with respect to the T conformation ($\Delta E = 1.05$ eV), as shown in Figure 4. The sulfur atom is in both cases on top of a gold atom, and the S−

Au distance is 2.51 Å for the H conformation and is almost the same for the T conformation (2.50 Å). The aromatic ring is quasi-coplanar for the T conformation, while it is tilted for the less stable H conformation. The tilt of the aromatic ring in the less stable geometry is due to a higher interaction of the oxygen atom with the gold surface: the distance of the oxygen atom from the surface along the normal to the plane is 2.40 Å for the H conformation, while in the T, the same quantity is 3.10 Å. In the H conformation, the oxygen atom is in a position between a top and a bridge arrangement, while for the T conformation, the oxygen atom is in an almost perfect bridge position with respect to the Au surface atoms (Au−O distance ∼3.4 Å). However, in H conformation, the smaller distance of the O atoms from the surface is not able to compensate for the lower interaction between the aromatic ring in H and the surface. This is the main reason for the 0.11 eV lower adsorption energy of the H with respect to the T conformation.

With respect to Metoso in the gas phase, it is calculated ($\delta_{PES(O\,1s)}$ in Figure 4) that Au(111) induces a shift of the binding energy of the core electron in the 1s orbital of the oxygen atom toward higher values (positive shift) for both the H and T conformations with a slightly greater shift ($\delta_{PES(O\,1s)}$ = +0.60 eV) for the H conformation since the O atom is about 0.5 Å nearer to the surface than the O atom of the T conformation ($\delta_{PES(O\,1s)}$ = +0.40 eV).

In Figure 4, the most stable structures of the Metoso$^{-CH_3}$ radical adsorbed on Au(111) are also shown. We denoted these structures H$^{-CH_3}$ and T$^{-CH_3}$. In T$^{-CH_3}$, the center of the aromatic ring is on top of an Au atom, while H$^{-CH_3}$ has the center of the aromatic ring on top of a hollow site. Both conformations have an adsorption energy ΔE = 0.97 eV, which is a value in between the adsorption energies of the two H and T conformations of Metoso.

The binding energy of the O 1s in T$^{-CH_3}$ and H$^{-CH_3}$ are shifted toward negative values with respect to the gas-phase Metoso ($\delta_{PES(O\,1s)}$ = −0.25 eV for T$^{-CH_3}$ and $\delta_{PES(O\,1s)}$ = −0.29 eV for H$^{-CH_3}$). This can be analyzed in terms of the polarization of the O−S bond. In fact, the Mulliken charges of Metoso and Metoso$^{-CH_3}$ in the gas phase indicate that the O−S bond is much more polarized in the molecule (qO = −0.73, qS = +0.91) than, for instance, the T$^{-CH_3}$ fragment (qO = −0.49, qS = +0.54), hence in the fragment there is less electron density on the O atom and less screening of the O nuclei which lowers the binding energy of its 1s electron.

When Metoso is adsorbed on the Au(111) surface, the calculated energy for the dissociation of the S−CH$_3$ bond, considering the reaction products (Metoso$^{-CH_3}$ and CH$_3$ radicals) both chemisorbed on Au(111), is −0.2 eV (−4.61 kcal/mol) for conformer T and −0.31 eV (−7.14 kcal/mol) for conformer H, as shown in Figure 5. Hence, at variance with the gas phase, on the Au(111) surface, the reaction is exothermic; it is yet more exothermic in the case of the less stable conformer H.

4. DISCUSSION

As reported in the previous paragraph, the S 2p PES spectra indicate the presence of two kinds of sulfur-containing species adsorbed on the Au(111) surface that can be assigned to the Metoso molecule and to the Metoso$^{-CH_3}$ radical resulting from the loss of a methyl group.

As shown in Figure 2c, the intensity of the S 2p core-level signal associated with the Metoso$^{-CH_3}$ radical (triangles in
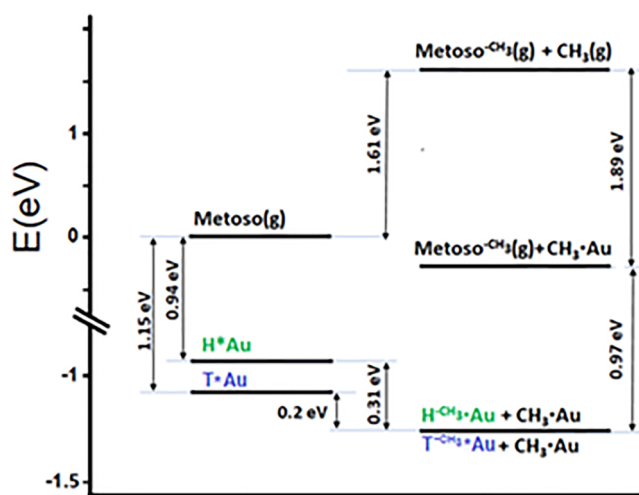
Figure 5. Born−Haber cycle resulting from the DFT-calculated energies for Metoso and fragments in gas phase and adsorbed on Au(111).

Figure 2c) increases with exposition, and, for both samples, continues to increase after the end of exposure. The increase of fragmentation with longer gas exposition can be also recognized taking into consideration the O 1s and C 1s signals.

The O 1s signal is broad and complex, due to the presence of various contributions from the intact molecules and fragments. The O 1s spectra have been fitted with four gaussian components (shown in Figure S4). Two components at 532.1 and 531.8 eV can be attributed to Metoso H and Metoso T and the component at 531.3 eV, shifted at lower BE values by −0.5 and −0.8 eV, can be attributed to the Metoso$^{-CH_3}$ fragment. In fact, the calculated O 1s shift between a single adsorbed Metoso molecule and a Metoso$^{-CH_3}$ radical (Figure 4) ranges between −0.65 and −0.89 eV, depending on the adsorption conformations of Metoso (H or T) and fragment (H$^{-CH_3}$ or T$^{-CH_3}$). A low peak area component, at higher BE values (533.2 eV) is attributed to impurities. The peak area of the component at 531.3 eV, attributed to the Metoso$^{-CH_3}$ fragment, results increased for the sample exposed for 60 min with respect to 30 min deposition. This effect can be associated, in accordance with the S 2p spectra, with the existence of additional Metoso$^{-CH_3}$ radicals present on the surface exposed to Metoso for a longer time.

The observed increase of the C 1s signal with time exposure (Figure 3b) is the signature of an increased amount of the total molecular species present on the surface. It can also be deduced that the methyl radical probably does not desorb from Au(111) in the time frame of the experiment since the increase of the C 1s signal at lower binding energy can be attributed to methyl radicals adsorbed on Au.[65] Indeed, the calculated adsorption energy of the methyl radical on the Au(111) surface is 1.89 eV (Figure 5), almost twice the adsorption energy of Metoso.

The curves reported in Figure 2c shows that the fraction of intact Metoso molecules present on the surface diminishes (τ ≈ 35 min) in vacuum, although after 2 h about 50% of the Metoso molecules remain on the surface, giving rise to a residual, almost constant signal for t >100 min. This experimental observation can be explained by considering that the total intensity of the Metoso signal is due to different adsorption conformations, showing different disappearance rates. Indeed, the Metoso molecules can adsorb on Au(111) in

different arrangements: the less stable conformation H or conformation T (see Figure 4). The ratio between the desorption rate constant of Metoso in the H (k_{-H}) and in the T (k_{-T}) conformations at room temperature can be estimated from the corresponding Arrhenius expressions, resulting in $k_{-H}/k_{-T} = e^{(\Delta E_{(T)} - \Delta E_{(H)}/K_B T)} = 77$, where $\Delta E_{(T)} - \Delta E_{(H)}$ is the adsorption energy difference between and T and H (Figure 4), K_B is the Boltzmann constant, and the preexponential factor in the Arrhenius expression is considered the same for T and H. This means that the more stable conformation T, at room temperature desorbs with a time rate that is about a factor of 77 slower than the rate of the H conformation. Another possible channel for the decrease in time of the total Metoso signal is the conversion into the Metoso$^{-CH_3}$ radical since the signal attributed to this radical slowly increases with time.

On the basis of the available experimental and theoretical data, we propose a simplified model, in which the fragmentation on the surface involving Metoso in the H and T conformations are considered independent of each other, as shown in Figure 6. In the model, we neglect the influence of aggregation between molecules adsorbed on the surface, though a similar model could also be extended to dimers or larger aggregates.
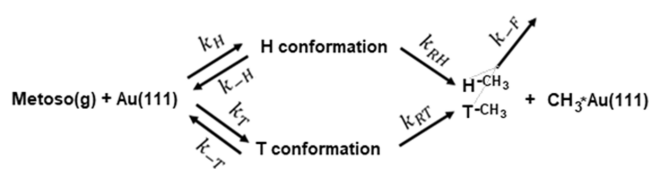

Figure 6. Proposed kinetic model.

In the kinetic scheme, k_H and k_T are the kinetic constants for the adsorption of Metoso in conformation H and T, respectively, while k_{-H} and k_{-T} are the kinetic constants for desorption. In this kinetic model, the reactions leading to Metoso$^{-CH_3}$ involve both H and T conformations, with k_{RH} and k_{RT} rate constants, respectively. k_{-F} is the rate constant for the desorption of Metoso$^{-CH_3}$ fragment, which, on the basis of calculated adsorption energies (Figure 4), is the same for H$^{-CH_3}$ and T$^{-CH_3}$. The model is based on the following assumptions: (i) recombination between the fragment and the methyl group is negligible in the timeframe of the experiment, that is, nonreversibility of the fragmentation reaction of Metoso; (ii) the desorption of the methyl radical is neglected since the calculated adsorption energy (1.89 eV) is high in comparison with Metoso and Metoso$^{-CH_3}$ (~1 eV); (iii) on the basis of the calculated DFT adsorption energies of H, T, H$^{-CH_3}$, and T$^{-CH_3}$ (Figure 4) $\frac{k_{-H}}{k_{-T}} \approx 77$ and $\frac{k_{-H}}{k_{-F}} \approx 3.3$; (iv) the assumption that the fragmentation on the surface involving H and T conformations are considered independent of each other implies that a possible conversion of conformer H into the most stable conformer T on the surface is neglected, although some comments on this point are reported in the Supporting Information.

In vacuum, ($k_H = 0$, $k_T = 0$), the solution of the system of rate equations of scheme 1 (see the Supporting Information) can be related to the area, normalized to the value at $t = 0$, of the S 2p signal ascribed to the molecules ($A_{Metoso}(t)/A_{Metoso}(t = 0)$) as a function of time, where $t = 0$ corresponds to the end of the adsorption process. The biexponential fit (see Figure

S5) provides three independent parameters: the total rate constants for the depletion of H ($k_{TH} = k_{-H} + k_{RH}$) and T ($k_{TT} = k_{-T} + k_{RT}$) conformations of Metoso from the Au(111) surface which are, in average, $k_{TH} = (26 \pm 7) \ 10^{-3} \ min^{-1}$ and $k_{TT} < (25 \pm 1) \ 10^{-5} \ min^{-1}$, and the fractional coverage (ρ) of H conformation, that is, the ratio between H and the total H + T conformations at time $t = 0$, $\rho = 0.49$ for 30 min deposition and $\rho = 0.44$ for 60 min deposition.

The low value of the k_{TT} constant is consistent with the fact that the desorption rate of T (k_{-T}) and the fragmentation of T (k_{RT}) are both much slower than the time frame of the experiment.

The peak area of the signal ascribed to the fragment as a function of time, normalized to the value at $t = 0$, ($A_{Metoso}-CH_3(t)/A_{Metoso}-CH_3(t = 0)$), have been employed to have a rough estimation of the rate constants for reaction and desorption of the H conformation, namely, in average $k_{RH} = 0.01 \pm 0.005 \ min^{-1}$ and $k_{-H} = 0.016 \pm 0.005 \ min^{-1}$, respectively. Use of the Arrhenius expression for k_{-H} at the temperature of the experiment with a DFT-calculated desorption energy of 0.94 eV results in a value of 4×10^{12} Hz for the surface bond vibration frequency.

The adsorption rate constant k_H can be estimated from the solution of the rate equations during exposure[66] as shown in the Supporting Information. In the quasi-steady-state approximation, we obtain $k_H = (6.6 \pm 4) \ 10^{-2} \ min^{-1}$.

5. CONCLUSIONS

The results described in this paper provide the first insight into the energetics and kinetics of an aromatic chiral sulfinyl compound deposited on Au(111) at room temperature. The Metoso molecule can adsorb on Au(111) in two different geometries depending on the position of the tolyl ring with respect to the surface atoms. At room temperature, the interaction with the Au(111) surface leads to a partial dissociation of the adsorbate with the formation of the p-tolyl sulfinyl radical. By means of combined experimental and theoretical approaches, we were able to estimate kinetic parameters related to the adsorption/desorption and reaction of the molecule on Au(111). The rate constants for desorption and reaction of the most stable adsorbed species were estimated to be smaller than the time frame of the experiment. An important parameter achieved from this study is the k_{RH} kinetic constant for the predominant reaction from the less stable conformer on the surface, leading to the p-tolyl sulfinyl radical, which results to be $0.010 \pm 0.005 \ min^{-1}$ at room temperature. Further investigations are planned in order to compare the present data with depositions at lower temperatures to obtain higher molecular coverages and to provide information for the kinetic analysis. We also plan to investigate racemic mixtures deposition of methyl p-tolyl sulfoxide on Au(111).

■ ASSOCIATED CONTENT

ⓈI Supporting Information

The Supporting Information is available free of charge at https://pubs.acs.org/doi/10.1021/acsomega.3c01647.

    Additional information on PES spectra in the S 2p, O 1s, and Au 4f regions; gas-phase PES spectra; description of surface coverage estimation; and rate equations (PDF)

◼ AUTHOR INFORMATION

Corresponding Author

Susanna Piccirillo − *Dipartimento di Scienze e Tecnologie Chimiche, Università di Roma "Tor Vergata", 00133 Rome, Italy; Istituto di Struttura della Materia-CNR (ISM-CNR), 00133 Rome, Italy;* ◉ orcid.org/0000-0002-7938-6852; Email: piccirillo@fisica.uniroma2.it

Authors

Mauro Satta − *Istituto per lo studio dei Materiali Nanostrutturati-CNR (ISMN-CNR), Department of Chemistry, Sapienza University of Rome, 00185 Rome, Italy*

Nicola Zema − *Istituto di Struttura della Materia-CNR (ISM-CNR), 00133 Rome, Italy*

Stefano Turchini − *Istituto di Struttura della Materia-CNR (ISM-CNR), 00133 Rome, Italy*

Stefano Franchi − *Istituto di Struttura della Materia-CNR (ISM-CNR), 00133 Rome, Italy*

Giorgio Contini − *Istituto di Struttura della Materia-CNR (ISM-CNR), 00133 Rome, Italy; Dipartimento di Fisica, Università di Roma "Tor Vergata", 00133 Rome, Italy*

Alessandra Ciavardini − *University of Nova Gorica, SI-5001 Nova Gorica, Slovenia; Istituto di Struttura della Materia-CNR (ISM-CNR), 34149 Trieste, Italy*

Cesare Grazioli − *Istituto Officina dei Materiali-CNR (IOM-CNR), 34012 Trieste, Italy*

Marcello Coreno − *Istituto di Struttura della Materia-CNR (ISM-CNR), 34149 Trieste, Italy*

Monica de Simone − *Istituto Officina dei Materiali-CNR (IOM-CNR), 34012 Trieste, Italy;* ◉ orcid.org/0000-0002-9491-0173

Massimo Tomellini − *Dipartimento di Scienze e Tecnologie Chimiche, Università di Roma "Tor Vergata", 00133 Rome, Italy*

Complete contact information is available at:
https://pubs.acs.org/10.1021/acsomega.3c01647

Notes

The authors declare no competing financial interest.

◼ ACKNOWLEDGMENTS

◼ REFERENCES

(1) Love, J. C.; Estroff, L. A.; Kriebel, J. K.; Nuzzo, R. G.; Whitesides, G. M. Self-Assembled Monolayers of Thiolates on Metals as a Form of Nanotechnology. *Chem. Rev.* **2005**, *105*, 1103−1169.

(2) Ulman, A. Formation and Structure of Self-Assembled Monolayers. *Chem. Rev.* **1996**, *96*, 1533.

(3) Singh, M.; Kaur, N.; Comini, E. Role of Self-Assembled Monolayers in Electronic Devices. *J. Mater. Chem. C* **2020**, *8*, 3938−3955.

(4) Casalini, S.; Bortolotti, C. A.; Leonardi, F.; Biscarini, F. Self-assembled monolayers in organic electronics. *Chem. Soc. Rev.* **2017**, *46*, 40.

(5) Habibi, N.; Kamaly, N.; Memic, A.; Shafiee, H. Self-assembled peptide-based nanostructures: Smart nanomaterials toward targeted drug delivery. *Nano Today* **2016**, *11*, 41−60.

(6) Zaera, F. Chirality in adsorption on solid surfaces. *Chem. Soc. Rev.* **2017**, *46*, 7374−7398.

(7) Ernst, K.-H. Molecular chirality at surfaces Karl-Heinz Ernst. *Phys. Status Solidi B* **2012**, *249*, 2057−2088.

(8) Contini, G.; Gori, P.; Ronci, F.; Cricenti, A.; Prosperi, T.; et al. Chirality transfer from a single chiral molecule to 2D superstructures in alaninol on the Cu(100) surface. *Langmuir* **2011**, *27*, 7410−7418.

(9) Speranza, M.; Rondino, F.; Satta, M.; Paladini, A.; Giardini, A.; Catone, D.; Piccirillo, S. Molecular and supramolecular chirality: R2PI spectroscopy as a tool for the gas-phase recognition of chiral systems of biological interest. *Chirality* **2009**, *21*, 119−144.

(10) Ciavardini, A.; Rondino, F.; Paladini, A.; Speranza, M.; Fornarini, S.; Satta, M.; Piccirillo, S. The effect of fluorine substitution on chiral recognition: interplay of CH···π, OH···π and CH···F interactions in gas-phase complexes of 1-aryl-1-ethanol with butan-2-ol. *Phys. Chem. Chem. Phys.* **2013**, *15*, 19360−19370.

(11) Irrera, S.; Contini, G.; Zema, N.; Sanna, S.; Prosperi, T.; et al. Two-dimensional chiral single domain by D-alaninol functionalization of Cu(100). *J. Phys. Chem. B* **2007**, *111*, 7478−7480.

(12) Gori, P.; Contini, G.; Prosperi, T.; Zema, N.; Palma, A.; et al. D-alaninol adsorption on Cu(100): Photoelectron spectroscopy and first-principles calculations. *J. Phys. Chem. B* **2008**, *112*, 3963−3970.

(13) Irrera, S.; Contini, G.; Zema, N.; Crotti, C.; Prosperi, T.; et al. Adsorption of d-alaninol on Cu(1 0 0). *Surf. Sci.* **2007**, *601*, 2562−2565.

(14) Contini, G.; Turchini, S.; Sanna, S.; Prosperi, T.; Zema, N.; et al. Transfer of chirality from adsorbed chiral molecules to the substrate highlighted by circular dichroism in angle-resolved valence photoelectron spectroscopy. *Phys. Rev. B* **2012**, *86*, No. 035426.

(15) Nuzzo, R. G.; Allara, D. L. Adsorption of bifunctional organic disulfides on gold surfaces. *J. Am. Chem. Soc.* **1983**, *105*, 4481−4483.

(16) Nuzzo, R. G.; Zegarski, B. R.; Dubois, L. H. Fundamental studies of the chemisorption of organosulfur compounds on gold(111). Implications for molecular self-assembly on gold surfaces. *J. Am. Chem. Soc.* **1987**, *109*, 733−740.

(17) Prime, K. L.; Whitesides, G. M. Self-Assembled Organic Monolayers: Model Systems for Studying Adsorption of Proteins at Surfaces. *Science* **1991**, *252*, 1164.

(18) Bain, C. D.; Troughton, E. B.; Tao, Y. T.; Evall, J.; Whitesides, G. M.; Nuzzo, R. G. *J. Am. Chem. Soc.* **1988**, *111*, 321−335.

(19) Dubois, L. H.; Zegarski, B. R.; Nuzzo, R. G. Molecular ordering of organosulfur compounds on Au(111) and Au(100): Adsorption from solution and in ultrahigh vacuum. *J. Chem. Phys.* **1993**, *98*, 678.

(20) Vericat, C.; Vela, M. E.; Benitez, G.; et al. Self-assembled monolayers of thiols and dithiols on gold: new challenges for a well-known system. *Chem. Soc. Rev.* **2010**, *39*, 1805−1834.

(21) Stammer, X.; Tonigold, K.; Bashir, A.; et al. A highly ordered, aromatic bidentate self-assembled monolayer on Au(111): a combined experimental and theoretical study. *Phys. Chem. Chem. Phys.* **2010**, *12*, 6445−6454.

(22) Contini, G.; Laajalehto, K.; Suoninen, E.; Marabini, A. M. 5-methyl-2-mercaptobenzoxazole adsorbed onto chalcocite (Cu2S): An XPS and X-AES study. *J. Colloid Interface Sci.* **1995**, *171*, 234−239.

(23) Di Castro, V.; Allegretti, F.; Baldacchini, C.; Betti, M. G.; Contini, G.; Corradini, V.; Lamastra, F.; Mariani, C. Growth of 2-mercaptobenzoxazole on Cu(100) surface: Chemisorbed and physisorbed phases. *Surf. Sci.* **2002**, *507−510*, 7−11.

(24) Contini, G.; Ciccioli, A.; Cozza, C.; Barbaro, M.; Marabini, A. M. Infrared study of 2-mercaptobenzothiazole and two of its derivatives adsorbed on PbS. *Int. J. Miner. Process.* **1997**, *51*, 283−291.

(25) Allegretti, F.; De Renzi, V.; Biagi, R.; del Pennino, U.; Contini, G.; Di Castro, V.; Mariani, C.; Betti, M. G.; Fontanesi, C. HREELS study of the adsorption mechanism and orientational order of 2-mercaptobenzoxazole on Cu(1 0 0). *Surf. Sci.* **2003**, *539*, 63−71.

(26) Colangelo, E.; Comenge, J.; Paramelle, D.; Volk, M.; Chen, Q.; Raphael, L. Characterizing Self-Assembled Monolayers on Gold Nanoparticles. *Bioconjugate Chem.* **2017**, *28*, 11−22.

(27) Zhang, X.; Du, X.; Huang, X.; Zhongpeng, L. Creating Protein-Imprinted Self-Assembled Monolayers with Multiple Binding Sites

and Biocompatible Imprinted Cavities. *J. Am. Chem. Soc.* **2013**, *135*, 9248−9251.

(28) Ielo, I.; Rando, G.; Giacobello, F.; Sfameni, S.; Castellano, A.; Galletta, M.; Drommi, D.; Rosace, G.; Plutino, M. R. Synthesis, Chemical−Physical Characterization, and Biomedical Applications of Functional Gold Nanoparticles: A Review. *Molecules* **2021**, *26*, 5823.

(29) Belser, T.; Stohr, M.; Pfaltz, A. Immobilization of Rhodium Complexes at Thiolate Monolayers on Gold Surfaces: Catalytic and Structural Studies. *J. Am. Chem. Soc.* **2005**, *127*, 8720−8731.

(30) Lukkari, J.; Meretoja, M.; Kartio, I.; Laajalehto, K.; Rajamaki, M.; Lindstro, M.; Kankare, J. Organic Thiosulfates (Bunte Salts): Novel Surface-Active Sulfur Compounds for the Preparation of Self-Assembled Monolayers on Gold. *Langmuir* **1999**, *15*, 3529−3537.

(31) Ciszek, J. W.; Tour, J. M. Mechanistic Implications of the Assembly of Organic Thiocyanates on Precious Metals. *Chem. Mater.* **2005**, *17*, 5684−5690.

(32) Houmam, A.; Muhammad, H.; Chahma, M.; Koczkur, K.; Thomas, D. F. 4-Nitrophenyl sulfenyl chloride as a new precursor for the formation of aromatic SAMs on gold surfaces. *Chem. Commun.* **2011**, *47*, 7095−7097.

(33) Koczkur, K. M.; Hamed, E. M.; Hesp, C. R.; Houmam, A. The intriguing reaction of aromatic sulfonyl phthalimides with gold surfaces. *Phys. Chem. Chem. Phys.* **2013**, *15*, 348.

(34) Dueñas-Mas, M. J.; Soriano, M. L.; Ruiz-Palomero, C.; Valcárcel, M. Modified nanocellulose as promising material for the extraction of gold nanoparticles. *Microchem. J.* **2018**, *138*, 379−383.

(35) Dishner, M. H.; Hemminger, J. C.; Feher, F. J. Formation of a self-assembled monolayer by adsorption of thiophene on Au(111) and its photooxidation. *Langmuir* **1996**, *12*, 6176−6178.

(36) Noh, J.; Ito, E.; Araki, T.; Hara, M. Adsorption of thiophene and 2,5-dimethylthiophene on Au(111) from ethanol solutions. *Surf. Sci.* **2003**, *532−535*, 1116−1120.

(37) Noh, J.; Ito, K.; Nakajima, J.; Kim, H.; Lee, M.; Hara, M. High-resolution STM and XPS studies of thiophene self-assembled monolayers on Au(111). *J. Phys. Chem. B* **2002**, *106*, 7139−7141.

(38) Jiang, T.; Malone, W.; Tong, Y.; Dragoe, D.; Bendounan, A.; Kara, A.; Esaulov, V. A. Thiophene Derivatives on Gold and Molecular Dissociation Processes. *J. Phys. Chem. C* **2017**, *121*, 27923−27935.

(39) Kiełbasiński, P.; Kwiatkowska, M.; Cierpia, T.; Rachwalskib, M.; Lesniak, S. The sulfinyl group: Its importance for asymmetric synthesis and biological activity. *Phosphorus, Sulfur, Silicon Relat. Elem.* **2019**, *194*, 649−653.

(40) Wojaczyńska, E.; Wojaczyński, J. Modern Stereoselective Synthesis of Chiral Sulfinyl Compounds. *Chem. Rev.* **2020**, *120*, 4578−4611.

(41) Prilezhaeva, E. N. Prilezhaeva Sulfones and sulfoxides in the total synthesis of biologically active natural compounds. *Russ. Chem. Rev.* **2000**, *69*, 367.

(42) Otocka, S.; Kwiatkowska, M.; Madalinska, L.; Kiełbasinski, P. Chiral Organosulfur Ligands/Catalysts with a Stereogenic Sulfur Atom: Applications in Asymmetric Synthesis. *Chem. Rev.* **2017**, *117*, 4147−4418.

(43) Schröter, C.; Roelfs, B.; Solomun, T. The Interaction of Dimethylsulfoxide with a Gold Surface. *Surf. Sci.* **1997**, *380*, L441−L445.

(44) Ikemiya, N.; Gewirth, A. A. Structure Sensitive Adsorption of DMSO on Au Surfaces. *J. Phys. Chem. B* **2000**, *104*, 873−877.

(45) Si, S. K.; Gewirth, A. A. Solvent Organization above Metal Surfaces: Ordering of DMSO on Au. *J. Phys. Chem. B* **2000**, *104*, 10775−10782.

(46) Roelfs, B.; Schröter, C.; Solomun, T. A Comparison of Metal/Vacuum and Metal/Electrolyte Interfaces: The Au(100)/(Dimethylsulfoxide) and (Dimethylsulfoxide P Acetonitrile) Systems. *Ber. Bunsen-Ges Phys. Chem.* **1997**, *101*, 1105−1112.

(47) Feng, Z.; Velari, S.; Cossaro, A.; Castellarin-Cudia, C.; Verdini, A.; Vesselli, E.; Dri, C.; Peressi, M.; De Vita, A.; Comelli, G. Trapping of Charged Gold Adatoms by Dimethyl Sulfoxide on a Gold Surface. *ACS Nano* **2015**, *9*, 8697−8709.

(48) Deng, L.; Mrksich, M.; Whitesides, G. M. Self-Assembled Monolayers of Alkanethiolates Presenting Tri(propylene sulfoxide) Groups Resist the Adsorption of Protein. *J. Am. Chem. Soc.* **1996**, *118*, 5136−5137.

(49) Bentley, R. Role of sulfur chirality in the chemical processes of biology. *Chem. Soc. Rev.* **2005**, *34*, 609−624.

(50) Dementyev, P.; Peter, M.; Adamovsky, S.; Schauermann, S. Chirally-modified metal surfaces: energetics of interaction with chiral molecules. *Phys. Chem. Chem. Phys.* **2015**, *17*, 22726−22735.

(51) Gellman, A. J.; Tysoe, W. T.; Zaera, F. Surface Chemistry for Enantioselective Catalysis. *Catal. Lett.* **2015**, *145*, 220−232.

(52) Ma, Y.; Shib, L.; Yuea, H.; Gao, X. Recognition at chiral interfaces: From molecules to cells. *Colloids Surf., B* **2020**, *195*, No. 111268.

(53) Bürgi, T. Properties of the gold−sulphur interface: from self-assembled monolayers to clusters. *Nanoscale* **2015**, *7*, 15553−15567.

(54) Myrseth, N. V.; Bozek, J. D.; Kukk, E.; Sæthre, L. J.; Thomas, T. D. Adiabatic and vertical carbon 1s ionization energies in representative small molecules. *J. Electron Spectrosc. Relat. Phenom.* **2002**, *122*, 57.

(55) Thomas, T. D.; Shaw, R. W. Accurate core ionization potentials and photoelectron kinetic energies for light elements. *J. Electron Spectrosc. Relat. Phenom.* **1974**, *5*, 1081.

(56) Siegbahn, K. *ESCA Applied to Free Molecules*; North-Holland: Amsterdam, 1971; p 94.

(57) Giannozzi, P.; Baroni, S.; Bonini, N.; Calandra, M.; Car, R.; Cavazzoni, C.; Ceresoli, D.; Chiarotti, G. L.; Cococcioni, M.; Dabo, I.; Corso, A. D.; de Gironcoli, S.; Fabris, S.; Fratesi, G.; Gebauer, R.; Gerstmann, U.; Gougoussis, C.; Kokalj, A.; Lazzeri, M.; Martin-Samos, L.; Marzari, N.; Mauri, F.; Mazzarello, R.; Paolini, S.; Pasquarello, A.; Paulatto, L.; Sbraccia, C.; Scandolo, S.; Sclauzero, G.; Seitsonen, A. P.; Smogunov, A.; Umari, P.; Wentzcovitch, R. M. QUANTUM ESPRESSO: a modular and open-source software project for quantum simulations of materials. *J. Phys.: Condens. Matter* **2009**, *21*, No. 395502.

(58) Liu, W.; Tkatchenko, A.; Scheffler, M. Modeling Adsorption and Reactions of Organic Molecules at Metal Surfaces. *Acc. Chem. Res.* **2014**, *47*, 3369−3377.

(59) Grimme, S. Semiempirical GGA-type density functional constructed with a long-range dispersion correction. *J. Comput. Chem.* **2006**, *27*, 1787−1799.

(60) Syomin, D.; Kim, J.; Koel, B. E.; Ellison, G. B. Identification of Adsorbed Phenyl (C6H5) Groups on Metal Surfaces: Electron-Induced Dissociation of Benzene on Au(111). *J. Phys. Chem. B* **2001**, *105*, 8387.

(61) Lavrich, D. J.; Wetterer, S. M.; Bernasek, S. L.; Scoles, G. Physisorption and Chemisorption of Alkanethiols and Alkyl Sulfides on Au(111). *J. Phys. Chem. B* **1998**, *102*, 3456−3465.

(62) Gong, J.; Flaherty, D. W.; Ojifinni, R. A.; White, J. M.; Mullins, C. B. Surface Chemistry of Methanol on Clean and Atomic Oxygen Pre-Covered Au(111). *J. Phys. Chem. C* **2008**, *112*, 5501−5509.

(63) Liu, G.; Rodriguez, J. A.; Dvorak, J.; Hrbek, J.; Jirsak, T. Chemistry of sulfur-containing molecules on Au(1 1 1): thiophene, sulfur dioxide, and ethanethiol adsorption. *Surf. Sci.* **2002**, *505*, 295−307.

(64) Cristina, L. J.; Ruano, G.; Salvarezza, R.; Ferrón, J. Thermal Stability of Self-Assembled Monolayers of n-Hexanethiol on Au(111)-(1 × 1) and Au(001)-(1 × 1). *J. Phys. Chem. C* **2017**, *121*, 27894−27904.

(65) Larciprete, R.; Goldoni, A.; Groŝo, A.; Lizzit, S.; Paolucci, G. The photochemistry of CH₄ adsorbed on Pt(1 1 1) studied by high resolution fast XPS. *Surf. Sci.* **2001**, *482−485*, 134−140.

(66) Tomellini, M. Modelling the kinetics of a gas-solid reaction involving a surface transient. *J. Chem. Soc., Faraday Trans.* **1993**, *89*, 3629.